chemosensors

MDPI

Article

A Simple but Efficient Voltammetric Sensor for Simultaneous Detection of Tartrazine and Ponceau 4R Based on TiO_2/Electro-Reduced Graphene Oxide Nanocomposite

Zirong Qin †, Jinyan Zhang †, Ying Liu, Jingtao Wu, Guangli Li *, Jun Liu and Quanguo He

College of Life Sciences and Chemistry, Hunan University of Technology, Zhuzhou 412007, China; qzrhut17@163.com (Z.Q.); zjyhut17@163.com (J.Z.); ly8931570@163.com (Y.L.); jtwu123@163.com (J.W.); junliu@hut.edu.cn (J.L.); hequanguo@126.com (Q.H.)

* Correspondence: guangli010@hut.edu.cn; Tel.: +86-189-7334-0268

† The authors contributed equally to this work.

Received: 17 July 2020; Accepted: 17 August 2020; Published: 19 August 2020

Abstract: In this work, we report a simple but efficient voltammetric sensor for simultaneous detection of ponceau 4R and tartrazine based on TiO_2/electro-reduced graphene oxide nanocomposites (TiO_2/ErGO). TiO_2/ErGO nanocomposites were prepared by ultrasonically dispersing TiO_2 nanoparticles (TiO_2 NPs) into graphene oxide (GO) solution followed by a green in-situ electrochemical reduction. TiO_2 NPs were uniformly supported on ErGO nanoflakes, which provides a favorable interface for the adsorption and subsequent oxidation of target analytes. TiO_2/ErGO showed remarkable electrocatalytic capacity for the oxidation of ponceau 4R and tartrazine, with minimized oxidation overpotentials and boosted adsorptive striping differential pulse voltammetric (AdSDPV) response peak currents. Under the optimal experimental conditions, the anodic peak currents of ponceau 4R and tartrazine increase linearly with the respective natural logarithm of concentrations from 0.01 to 5.0 μM. The detection limits (LOD = 3σ/s) for ponceau 4R and tartrazine are 4.0 and 6.0 nM, respectively. The extraordinary analytical properties of TiO_2/ErGO/GCE are primarily attributed to the synergistic enhancement effect from ErGO nanoflakes and TiO_2 NPs. Moreover, the proposed TiO_2/ErGO/GCE achieves reliable determination of ponceau 4R and tartrazine in orange juice with excellent selectively, reproducibility and stability. Together with simplicity, rapidness, and low cost, the proposed sensor demonstrates great potential for on-site detection of azo colorants.

Keywords: ponceau 4R; tartrazine; TiO_2; electro-reduced graphene oxide; voltammetric sensor

1. Introduction

As two typical edible synthetic azo colorants, ponceau 4R and tartrazine always coexist together to give the orange color to food like orange juice. Due to their outstanding advantages such as relatively lower price, good water-solubility, low microbiological contamination and high stability, ponceau 4R and tartrazine have been widely added to make foodstuffs more appealing and appetizing [1]. However, ponceau 4R and tartrazine contain poisonous and carcinogenic aromatic ring structures and azo functional groups (–N=N–). Therefore, ponceau 4R and tartrazine likely lead to many adverse health effects such as allergies, neurobehavioral toxicities and cancers if they are excessively consumed [2–4]. To guarantee food safety, the dosages of ponceau 4R and tartrazine have been severely restricted by laws and regulations. For example, the joint FAO/WHO Expert Committee on Food Additives (JECFA) has set the acceptable daily intake (ADI) for ponceau 4R and tartrazine as 4.0 and 7.5 mg/kg bw/day, respectively [5,6]. In China, the maximum permitted dosages for ponceau 4R and

tartrazine in non-alcoholic beverages should not be more than 0.1 mg/mL (GB 2760–2007). Hence, the development of low cost but efficient analytical techniques for the sensitive determination of ponceau 4R and tartrazine is essential for food safety and human health.

Currently, several analytical techniques have been developed for simultaneous detection of ponceau 4R and tartrazine, including capillary electrophoresis [7,8], spectrophotometry [9,10] and high-performance liquid chromatography [11–13]. These analytical methods are widely accepted and well proved, but they usually involve tedious and time-consuming analytical procedures and require costly equipment and high consumption of organic solvents. Owing to its low price, simple operation, excellent sensitivity and ease of miniaturization, the electroanalytical technique has recently been regarded as a competitive candidate for the in situ determination of azo colorants. Due to the presence of electrochemically active –N = N– groups, ponceau 4R and tartrazine can be readily detected by mercury electrodes based on their reduction signals [14–16]. However, the use of toxic mercury electrodes can inevitably cause adverse health effects and environmental pollution. Alternatively, a variety of mercury-free electrodes was fabricated for the individual determination of ponceau 4R [17–19] and tartrazine [20–23]. As far as we know, there are very few electrochemical sensors for simultaneous detection of ponceau 4R and tartrazine. Yang et al. [24] constructed an acetylene black film modified electrode for the simultaneous determination of ponceau 4R and tartrazine, but the proposed sensor suffered from lower sensitivity and inadequate detection limits (LODs). Ionic liquid modified expanded graphite paste electrode (IL-EGPE) [25] and ionic liquid-graphene oxide-multiwalled carbon nanotube nanocomposite (IL-GO-MWCNT) [26] showed extraordinary electrocatalytic oxidation capacity toward ponceau 4R and tartrazine. However, costly ionic liquids enormously hinder their practical applications. In our previous studies, TiO_2/graphene nanocomposites exhibited high catalytic activity for tartrazine electrooxidation [27]. However, to the best of our knowledge, TiO_2/graphene nanocomposite-based voltammetric sensors have not been used for simultaneous determination of ponceau 4R and tartrazine yet. Therefore, designing voltammetric sensors with simplicity, cost-effectiveness and excellent sensitivity is paramount for simultaneous determination of ponceau 4R and tartrazine.

TiO_2 nanoparticles (NPs) have been considered as the most promising candidate for advanced (photo)electrochemical sensors, owing to their attractive advantages such as more abundance, low cost, high electrical conductivity, strong adsorptive ability and remarkable catalytic activity [28–32]. However, TiO_2 NPs cannot be firmly immobilized on the surface of carbon electrodes [33], thereby deteriorating electrode stability and sensing property. In addition, TiO_2 NPs tend to aggregate without surfactant as a dispersant, which also degrades sensing performance. In order to address these issues, TiO_2 NPs are often anchored on the graphene to improve the dispersibility and immobilization of TiO_2 NPs onto carbon electrodes. Considering the advantageous features including huge specific surface area, excellent electroconductivity and extraordinary electron transfer capacity, graphene has become a versatile material to construct electrochemical sensing platforms [34–39]. Graphene with unique two-dimensional layered structures and intriguing electronic properties provide a favorable catalyst carrier for anchoring metal oxide nanoparticles [40], therefore achieving versatile selective catalytic or sensing performance. In addition, graphene can be readily anchored on the GCE surface through π–π interactions. For these reasons, TiO_2/graphene nanocomposites have been exploited as efficient sensing films for voltammetric determination of biomolecules such as guanine [31], adenine [31], dopamine [41], glucose [42], L-tyrosine [43] and L-tryptophan [43]. However, to the best of our knowledge, TiO_2/graphene nanocomposite-based voltammetric sensors have not been used for the simultaneous determination of ponceau 4R and tartrazine yet.

Herein, a simple but efficient voltammetric sensor was designed for simultaneous determination of ponceau 4R and tartrazine in orange juice based on TiO_2/ErGO. TiO_2/ErGO nanocomposites were prepared by ultrasonically dispersing TiO_2 NPs into graphene oxide (GO) solution followed by a green in-situ electrochemical reduction. TiO_2 NPs were uniformly supported on ErGO nanoflakes, which provide a favorable interface for the adsorption and subsequent oxidation of target analytes. The resultant TiO_2/ErGO generated synergistic effect toward the electrooxidation of ponceau 4R and

tartrazine, which gives arise to amplified response signals. Furthermore, the proposed sensor was used for simultaneous determination of Ponceau 4R and Tartrazine in orange juice sample with satisfactory outcomes.

2. Materials and Methods

2.1. Chemicals and Materials

Ponceau 4R, tartrazine, Allura Red, amaranth and sunset yellow were bought from Aladdin Reagents Inc. (Shanghai, China). Other chemicals were supplied by Sinopharm Chemical Reagent Co., Ltd. (Shanghai, China). All chemicals were directly used without further treatments. GO was supplied by Xianfeng Nanomaterial Technology Inc. (Nanjing, China). Orange juice samples were purchased from a local supermarket. Deionized water from a Millipore water purification system (Mini-Q, 18 MΩ cm) was used throughout the experiments.

2.2. Synthesis of TiO_2 NPs

TiO_2 NPs were prepared by a facile hydrothermal treatment. In a typical procedure, 2.4034 g of titanium sulfate were dissolved into 50 mL of deionized water, and then subjected to ultrasonication for 40 min. Afterwards, the reaction solution was transferred into a 100 mL Teflon-lined stainless-steel container and heated at 180 °C for 4 h. After being cooled into ambient temperature naturally, the resultant solution was centrifuged at 12,000 rpm for 15 min, and the supernatant was decanted gently. The as-collected white solid was alternately rinsed three times with absolute ethanol and deionized water, and then allowed to dry at 60 °C overnight.

2.3. Synthesis of TiO_2/GO Nanocomposites

Firstly, 0.2000 g of GO was dispersed into 10 mL deionized water under ultrasonication for 1 h to form a uniform GO dispersion (20 mg/mL). Then 0.0100 g TiO_2 NPs were added into 10 mL GO dispersion and ultrasonically dispersed for 1 h to get a homogenous TiO_2/GO dispersion.

2.4. Preparation of TiO_2/ErGO/GCE

Bare glass carbon electrode (GCE, diameter of 3 mm, GAOSSUNION, Tianjin, China) was polished to a shiny mirror-like surface with 0.05 μm Al_2O_3 powder. Then the GCE was alternately rinsed three times by absolute ethanol and deionized water under ultrasonication (each for 1 min), and was dried with an exposure of infrared light. TiO_2/ErGO nanocomposite modified electrode (TiO_2/ErGO/GCE) was fabricated by a convenient drop-casting technique followed by an in-situ potentiostatic reduction. In brief, 5 μL of TiO_2/GO dispersion was firmly coated on the surface of the freshly polished GCE, and then allowed to form an intact sensing film with the radiation of an infrared light. Afterwards, the as-obtained TiO_2/GO/GCE was immersed into 0.1 M phosphate buffer solution (PBS, pH 7.0), then electrochemically reduced into TiO_2/ErGO/GCE at −1.5 V for 2 min with stirring.

2.5. Voltammetric Determination of Ponceau 4R and Tartrazine

All voltammetric measurements were implemented on a CHI 760E electrochemical workstation (Chenhua Inc., Shanghai, China) with a typical three-electrode setup. A bare or modified electrode was used as the working electrode. A saturated calomel electrode (SCE) and a platinum wire were served as the reference electrode and auxiliary electrode, respectively. Unless otherwise specified, 0.1 M PBS (pH 7.0) was used as the supporting electrolyte. The electrochemical properties of different electrodes were studied by cyclic voltammetry and AC impedance spectra in 0.1 M KCl solution containing 5 mM $[Fe(CN)_6]^{3-/4-}$ probe. Cyclic voltammograms of different electrodes were recorded over the range of −0.2 – 0.6 V at a speed of 0.1 V s^{-1}. AC impedance spectra were measured at open circuit potential from 100 kHz to 0.1 Hz with 5 mV (rms) AC sinusoid signal. To boost the voltammetric responses, a suitable deposition was applied before the voltammetric measurements. Considering its

advantageous features of superior resolution and sensitivity, differential pulse voltammetry (DPV) was used for the simultaneous determination of ponceau 4R and tartrazine. The pulse amplitude, pulse width, sample width and pulse period for the DPV recording were set at 0.05 V, 0.05 s, 0.02 s and 0.2 s, respectively.

3. Results and Discussions

3.1. Physical Chararazation of TiO_2/ErGO

The TEM images of TiO_2 NPs and TiO_2/GO are shown in Figure 1A,B. TiO_2 NPs shows cube-like structures with the size of ca. 30~45 nm (Figure 1A). A large proportion of TiO_2 NPs is uniformly and compactly embedded on the GO substrates without notable aggregation (Figure 1B). It can be seen from the TEM image of TiO_2/GO that a great quantity of TiO_2 NPs is attached onto the surface of GO nanoflakes. It was reported that GO is heavily oxygenated, bearing carboxyl groups at its basal edges and epoxide or hydroxyl groups on the basal planes [44]. On one hand, GO functions as an amphiphilic surfactant to enhance the dispersion of TiO_2 NPs, due to the presence of massive hydrophilic oxygen-containing functional groups (OxFGs) on the hydrophobic basal planes [45]. On the other hand, OxFGs promote the intercalation of Ti species into GO layers via interaction with the hard Ti^{4+} Lewis acid [46,47]. Highly dispersed TiO_2 NPs on supports with large surface area GO would be conducive to enhance catalytic activity [30] and sensor sensitivity [48]. GO can be electrochemically reduced into ErGO with in-situ anchoring TiO_2 NPs on the resultant graphene flakes.

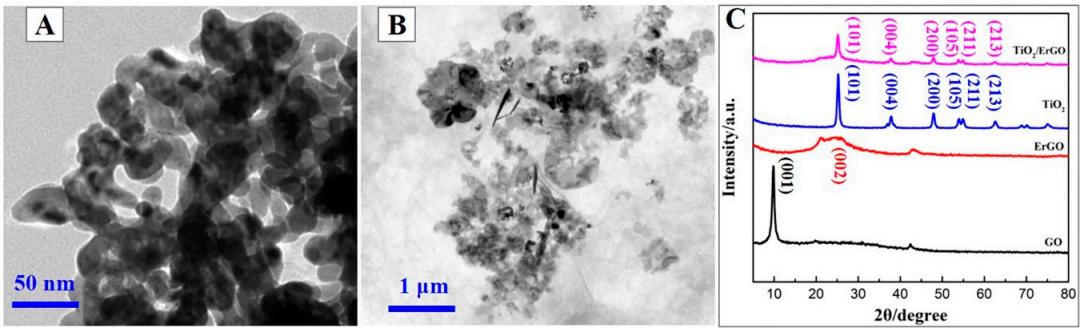

Figure 1. TEM images of TiO_2 nanoparticles (NPs) (**A**) and TiO_2/GO nanocomposites (**B**); (**C**) XRD patterns of GO, ErGO, TiO_2 and TiO_2/ErGO nanocomposites.

The crystalline structures of GO flakes, ErGO flakes, TiO_2 NPs and TiO_2/GO nanocomposites were examined by X-ray diffraction (XRD). As depicted in Figure 1C, GO exhibited a sharp and distinct diffraction peak at the 2θ of 9.8°, attributing to the (001) facet. After the electrochemical reduction of GO, the (001) facet completely disappeared, and a new broad diffraction peak occurred around 24° that corresponded to the (002) facet. This suggests an increase in the graphitic nature of ErGO because of the decreased interlayer spacing to 3.55 Å after electrochemical reduction. The broad diffraction peak indicates the loss of crystallinity in graphite. After incorporation of TiO_2 NPs into ErGO nanoflakes, the feature peak of ErGO (broad peak around 24°) can be also recognized. In addition, apparent diffraction peaks were observed at 25.26°, 36.92°, 47.94°, 53.98°, 54.90° and 62.60°, respectively, which can be assigned to the anatase TiO_2 NPs supported on ErGO substrates as (101), (004), (200), (105), (211) and (213) crystal planes (tetragonal, JCPDS 21-1272). In addition, no any evident impurity diffraction peaks are found, which demonstrates that the as-prepared TiO_2/ErGO nanocomposites are of high purity.

3.2. Electrochemical Properties of TiO_2/ErGO

Figure 2A shows cyclic voltammograms of various electrodes in 0.1 M KCl solution containing 5 mM $[Fe(CN)_6]^{3-/4-}$. Obviously, a pair of well-shaped and symmetrical redox peaks occurred at all

electrodes with the anodic/cathodic peak current ratio (I_{pa}/I_{pc}) of 1.0 approximately, demonstrating that the redox behavior of Fe^{III}/Fe^{II} corresponded to a quasi-reversible process. At bare GCE, a pair of relative weak redox peaks (I_{pa} = 99.27μA; I_{pc} = 99.90 μA) appeared at 0.266 and 0.121 V, respectively. After loading of TiO_2 NPs onto the GCE surface, the I_{pa} and I_{pc} increased to 125.1 and 119.5 μA while the peak separation (ΔE_p) decreased from 0.145 to 0.109 V. This phenomenon indicates TiO_2 NPs own electrocatalytic capacity. Likewise, the I_{pa} and I_{pc} also increased (I_{pa} = 137.3 μA; I_{pc} = 137.5 μA) on the ErGO modified electrode meanwhile the ΔE_p declined to 0.101 V, which suggests that ErGO nanoflakes accelerated an electron transfer process significantly due to its good electrical conductivity and high specific surface area. As expected, the best voltammetric responses (I_{pa} = 148.2 μA; I_{pc} = 144.1 μA) were achieved at TiO_2/ErGO/GCE with minimized ΔE_p (0.097 V), mainly due to the synergistic effect from ErGO nanoflakes and TiO_2 NPs. Based on the Randles–Sevcik equation [36,49], the electroactive surface areas of bare, TiO_2 NPs, ErGO nanoflakes and TiO_2/ErGO modified GCEs were calculated as 0.072, 0.084, 0.10 and 0.13 cm^2, respectively. TiO_2/ErGO nanocomposites greatly enlarged the electroactive surface area, which could provide more available reactive active sites for the adsorption and oxidation of azo colorants, thus ultimately boosting the voltammetric responses.

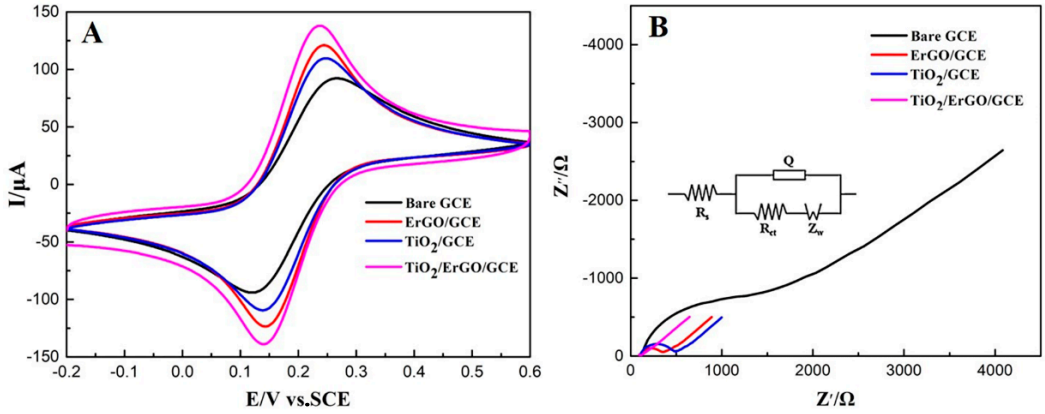

Figure 2. Cyclic voltammograms (**A**) and Nyquist plots (**B**) recorded at various electrodes in 0.1 M KCl solution (pH 7.0) containing 5 mM $[Fe(CN)_6]^{3-/4-}$. The inset in Figure 2B represents the equivalent circuit model for impedance fitting.

AC impedance spectra have become the most popular technique to acquire the electrode interfacial characteristic [36,49–51]. Nyquist plots of different electrodes are illustrated in Figure 2B. Typically, the diameter of semicircle is equivalent to the charge transfer resistance (R_{ct}). The largest semicircle was observed at bare GCE (R_{ct} = 1562 Ω), indicating sluggish electrode kinetics occurred at the unmodified electrode. After decoration with TiO_2 NPs and ErGO nanoflakes, the R_{ct} value decreased to 366 Ω and 233 Ω, respectively, indicating that TiO_2 NPs or ErGO nanoflakes promoted the electron transfer efficiently. The Nyquist plot of TiO_2/ErGO/GCE was almost a straight line, which demonstrates that the TiO_2/ErGO nanocomposite minimizes the R_{ct} value (R_{ct} = 44.9 Ω). This is primarily attributed to the fact that the synergistic effect from ErGO nanoflakes and TiO_2 NPs expedites the electron transfer. It is believed that the significant reduction in R_{ct} is a benefit to improve the sensor sensitivity.

3.3. Enrichment in Voltammetric Responses of Ponceau 4R and Tartrazine

The voltammetric responses of 1.0 μM ponceau 4R and tartrazine were investigated in 0.1 M PBS (pH 7.0). Figure 3 shows the DPV curves of 1.0 μM ponceau 4R and tartrazine (1:1) at different modified electrodes. At the bare electrode, two weak and ill-shaped anodic peaks appeared at 0.628 and 0.872 V, corresponding to the oxidation of ponceau 4R and tartrazine. In this case, the anodic peak currents of ponceau 4R and tartrazine were 0.327 and 0.0540 μA, respectively. After loading TiO_2 NPs alone, the anodic peak currents of ponceau 4R and tartrazine increased to 0.383 and 0.176 μA, respectively. The poor voltammetric responses of ponceau 4R and tartrazine are attributed to the

offset effect between their poor dispersibility and excellent electrocatalytic capacity [31,41,42,52]. Two well-shaped and pronounced anodic peaks occurred at ErGO nanoflakes modified electrodes. In addition, the voltammetric responses of ponceau 4R and tartrazine boost significantly, with their respective anodic peak currents of 0.418 and 1.21 μA, respectively. This may be strongly benefited from the intrinsic properties of ErGO nanoflakes such as a large surface area and high conductivity, which promote the absorption and subsequent electrooxidation of azo colorants effectually [52]. When loading TiO_2/ErGO onto the GCE surface, two sharp and well-defined anodic peaks occurred at 0.616 and 0.868 V, respectively. Moreover, the voltammetric responses of ponceau 4R and tartrazine enhanced prominently, with their respective anodic peak currents of 2.03 and 0.541 μA, respectively. The anodic peak currents of ponceau 4R and tartrazine were 5-fold and 9-fold higher as compared to bare GCE, respectively. The lowered oxidation overpotentials and remarkably enhanced peak currents suggest that TiO_2/ErGO nanocomposites generated the conspicuous synergistic effect toward the electrooxidation of ponceau 4R and tartrazine. To be specific, the excellent adsorption capability and electrocatalytic effect of TiO_2/ErGO nanocomposites greatly improve electron transfer efficiency, thus ultimately amplifying the voltammetric responses [31,41–43,52]. In addition, the high electrochemical active area and low charge transfer resistance also contributed to the extraordinary electrocatalytic performances.

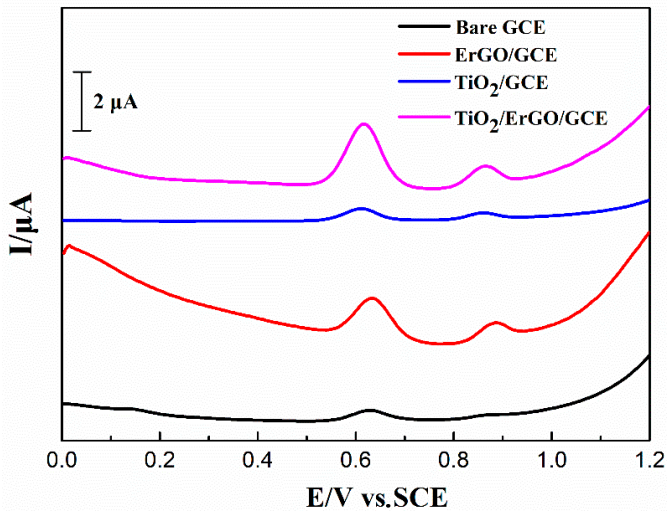

Figure 3. Differential pulse voltammetry (DPV) curves of 1.0 μM ponceau 4R and tartrazine (1:1) at different modified electrodes. Supporting electrolyte: 0.1 M PBS (pH = 7.0); deposition parameters: −0.1 V, 120 s.

3.4. Exploration of Voltammetric Parameters

3.4.1. Deposition Parameters

Deposition parameters directly determine the voltammetric responses of ponceau 4R and tartrazine. Therefore, the dependences of deposition potential as well as time on the voltammetric responses were also investigated. Both the anodic peak current of ponceau 4R and tartrazine (I_{pa}(PR) and I_{pa}(TZ)) increased gradually as the deposition potentials moved from −0.4 to −0.1 V, then reached maximum values at −0.1 V, afterwards it sharply decreased with more positive potentials (Figure 4A). Likewise, both I_{pa}(PR) and I_{pa}(TZ) sharply increased within the first 120 s, then they decreased dramatically as the deposition time exceeded 120 s (Figure 4B). So, the optimal deposition parameters were −0.1 V, 120 s.

3.4.2. Medium pH

Figure 5A displays the DPV curves of ponceau 4R and tartrazine at various medium pH. The anodic peaks of ponceau 4R and tartrazine shifted negatively as medium pH increased,

demonstrating that the redox reactions of ponceau 4R and tartrazine involve protons (H^+). Furthermore, the anodic peak potentials of ponceau 4R and tartrazine were inversely proportional to medium pH (Figure 5B). Their corresponding linear equations were E_{pa} (V) = −0.0676pH + 1.38 (R^2 = 0.986) and E_{pa} (V) = −0.0474pH + 0.892 (R^2 = 0.989) for ponceau 4R and tartrazine, respectively. Their respective slopes (67.6 and 47.4 mV/pH) closely approached the Nernstian values (59 mV/pH), implying that the numbers of electrons (e^-) and protons (H^+) was 1:1. Besides, both I_{pa} (PR) and I_{pa} (TZ) increased gradually as the medium pH increased from 5.8 to 7.0, then they suddenly reduced when medium pH was beyond 7.0 (Figure 5C). So, the optimal pH was set at 7.0.

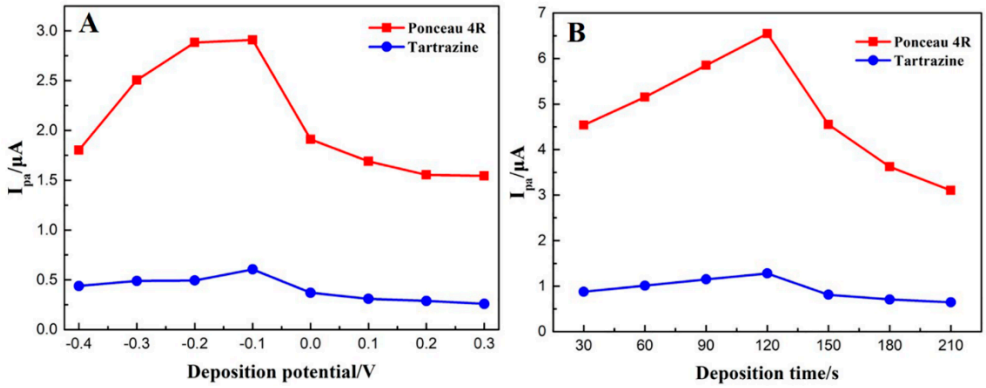

Figure 4. Effect of deposition potential (**A**) and deposition time (**B**) on the DPV anodic peak currents of ponceau 4R and tartrazine. (A) Deposition time was set at 150 s and (B) deposition potential was fixed at −0.1 V.

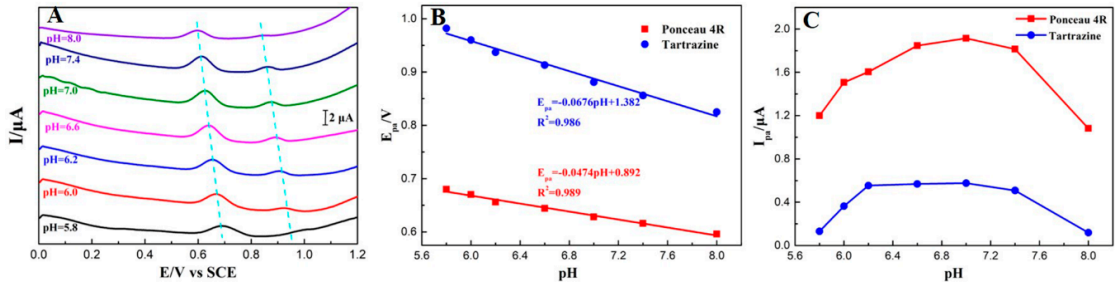

Figure 5. (**A**) DPV curves of ponceau 4R and tartrazine on TiO_2/ErGO/GCE measured at different pH; (**B**) the dependence of anodic peak potential of ponceau 4R and tartrazine on pH and (**C**) the dependence of anodic peak current of ponceau 4R and tartrazine on pH. Deposition parameters: −0.1 V, 120 s.

3.4.3. Scan Rate

Cyclic voltammograms of ponceau 4R and tartrazine at various scan rates are illustrated in Figure S1. The symmetric redox peaks of ponceau 4R suggest that ponceau 4R underwent a quasi-reversible process. In contrast, no cathodic peak of tartrazine was found at the reverse scan, indicating tartrazine underwent a totally irreversible process. Notably, both I_{pa} (PR) and I_{pa} (TZ) increased steadily as the scan rates increased from 0.03 to 0.3 Vs^{-1}. In addition, the redox peak currents of ponceau 4R and tartrazine (I_{pa} or I_{pc}) increased linearly with the square root of scan rates (Figure 6A,B), suggesting the reactions of ponceau 4R and tartrazine are typical diffusion-controlled processes. As the potential scan rate grew up, the anodic peaks shifted positively while the cathodic peaks moved towards the reverse direction. The redox peak potentials (E_{pa} or E_{pc}) were highly correlated with natural logarithm of scan rates (Figure 6C,D). According to Laviron theory [53], the slope values of E_{pa}-ln$v$ and E_{pc}-ln$v$ plots are equivalent to RT/2αnF. Generally, α is assumed as 0.5 for a quasi-reversible or irreversible electrode reaction. Therefore, the electron transfer number (n) was estimated to 0.95 (≈1)

and 1.19 (≈1) for ponceau 4R and tartrazine, respectively, implying one electron participation in the electrooxidation of ponceau 4R and tartrazine. Therefore, it can be inferred that the electrooxidation mechanisms of ponceau 4R and tartrazine involved one electron (1 e^-) transfer coupled with one proton (1 H^+). The possible electrooxidation mechanisms are illustrated in Figure 7. On the TiO_2/ErGO/GCE, the hydroxyl groups in ponceau 4R and tartrazine were oxidized to carbonyl groups with releasing 1 e^- and 1 H^+, which are in good agreement with the previous reports [19,20,22,54].

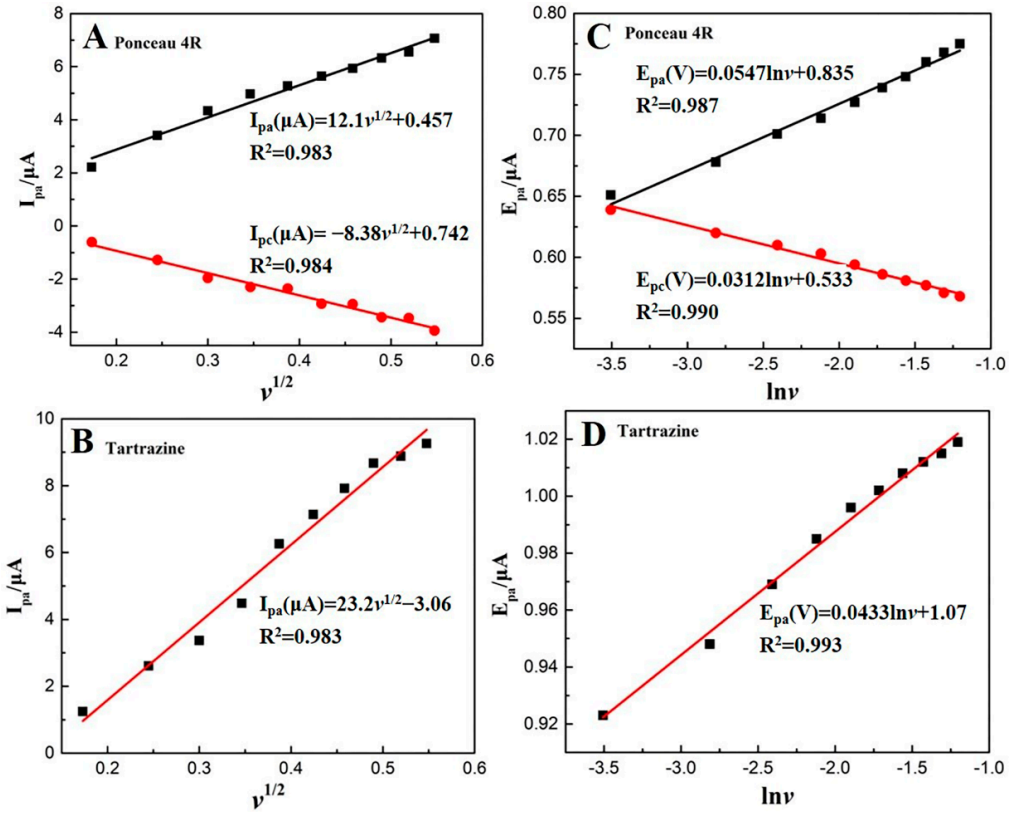

Figure 6. Linear plots of cyclic voltammograms peak currents of ponceau 4R (**A**) and tartrazine (**B**) against the square root of the scan rate ($v^{1/2}$) and linear plots of redox peak potentials of ponceau 4R (**C**) and tartrazine (**D**) against the natural logarithm of the scan rate (ln v).

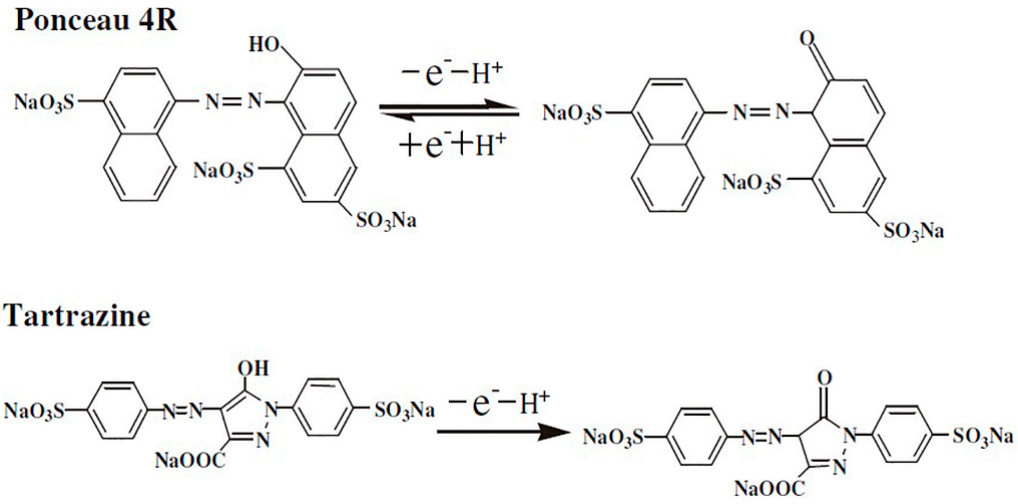

Figure 7. Electrooxidation mechanism of ponceau 4R and tartrazine at TiO_2/ErGO/GCE.

3.5. Determination of Ponceau 4R and Tartrazine

Figure 8A shows the DPV curves of ponceau 4R and tartrazine with their concentrations changing from 0.01 to 5.0 μM. Apparently, the response anodic peak currents of ponceau 4R and tartrazine increased gradually as their corresponding concentrations. In the concentration range from 0.01 to 5.0 μM, both I_{pa}(PR) and I_{pa}(TZ) increased linearly with the respective natural logarithm of concentrations (Figure 8B,C). The linear functions of I_{pa}−lnC can be expressed as I_{pa}(μA) = 0.150 lnC (μM) + 1.22 (R^2 = 0.991) and I_{pa}(μA) = 0.0774 lnC (μM) + 0.386 (R^2 = 0.991) for ponceau 4R and tartrazine, respectively. It is noted that both I_{pa}(PR) and I_{pa} (TZ) also increased linearly with their respective concentrations at the low concentration domain (0.01~0.3 μM). The corresponding linear regression equations of ponceau 4R and tartrazine were I_{pa}(μA) = 0.290C (μM) + 0.608 (R^2 = 0.989) and I_{pa}(μA) = 0.165C (μM) + 0.0505 (R^2 = 0.986), respectively. At higher concentration, the linear relationship changed to a semi-log relationship, probably because more ponceau 4R and tartrazine molecules were adsorbed on the electrode surface at high concentrations, which reduced the reversibility of the redox of ponceau 4R and tartrazine, thereby resulting in a sluggish electrode kinetics. The LODs (LOD = 3σ/s) for the determination of ponceau 4R and tartrazine were estimated to 4.0 and 6.0 nM, respectively. As summarized in Table 1, the sensing properties (including dynamics response range and LOD) were almost comparable or even exceeded previously reported electrodes. Unlike costly ionic liquids [25,26], the electrode preparation only involves readily available and low cost raw materials. Compared with aluminum microfiber/CPE and porous carbon-2/GCE [54,55], the fabrication of the proposed TiO_2/ErGO/GCE was simpler and more convenient. In short, the comparatively excellent sensing performances, together with low cost and ease of fabrication, make TiO_2/ErGO/GCE an attractive candidate for on-site detection of ponceau 4R and tartrazine.

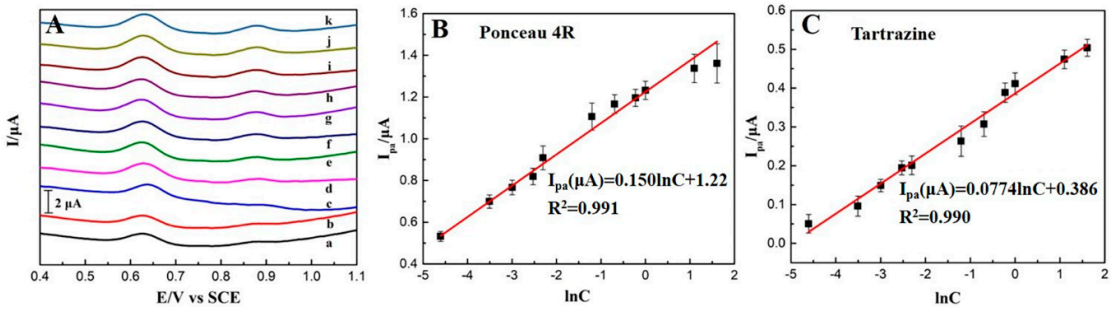

Figure 8. (**A**) DPV curves of ponceau 4R and tartrazine with their concentrations varying from 0.01 to 5.0 μM, a→k: 0.01, 0.003, 0.05, 0.08, 0.10, 0.30, 0.50, 0.80, 1.0, 3.0 and 5.0 μM; (**B**) plots of the anodic peak currents of ponceau 4R as the function of the natural logarithm of its concentrations in the range of 0.01–5.0 μM (n = 3) and (**C**) plots of the anodic peak currents of tartrazine as the function of natural logarithm of its concentrations in the range of 0.01–5.0 μM (n = 3).

Table 1. Comparison on analytical performance of the simultaneous detection of ponceau 4R and tartrazine with previously reported electrodes.

Electrode	Method	Detection Range (μM)		LOD (μM)		Ref
		Ponceau 4R	Tartrazine	Ponceau 4R	Tartrazine	
Acetylene black/GCE	AASV	0.083–6.6	0.28–34	0.050	0.187	[24]
IL-EGPE	SWSV	0.01–5.0	0.01–2.0	0.0014	0.003	[25]
IL-GO/MWCNT/GCE	SWV	0.008–0.015	0.02–0.013	0.006	0.01	[26]
Al microfiber/CPE	DPV	0.001–0.10	0.005–0.14	0.0008	0.002	[54]
Porous carbon-2/GCE	DPV	0.004–1.65	0.009–0.56	0.0035	0.0065	[55]
TiO_2/ErGO/GCE	AdSDPV	0.01–5.0	0.01– 5.0	0.004	0.006	This work

3.6. Interference, Reproducibility and Stability Test

The interferences from common metal ions and other azo colorants were investigated at the TiO_2/ErGO/GCE for the simultaneous determination of ponceau 4R and tartrazine. The anodic peak currents of 10 μM ponceau 4R and tartrazine coexisting with various interfering substances are tabulated in Table S1. The DPV responses of ponceau 4R and tartrazine were not influenced by the additions of 100-fold concentrations of Na^+, K^+, Mg^{2+} and Ca^{2+} or 10-fold concentrations of sunset yellow, Allura Red and amaranth. This indicates that it is feasible to analyze ponceau 4R and tartrazine at TiO_2/ErGO/GCE with high selectivity. To examine the electrode reproducibility, the DPV responses of 10 μM ponceau 4R and tartrazine were parallelly recorded on five TiO_2/ErGO/GCEs (Figure S2). The relative standard deviations (RSD) for ponceau 4R and tartrazine were 5.04% and 4.01%, respectively, indicating that the electrode preparation was highly reproducible. To evaluate electrode stability, the DPV responses of ponceau 4R and tartrazine were regularly monitored during one week. When it was not in use, the TiO_2/ErGO/GCE was stored in the air. After each measurement, the adsorbed target analytes on the TiO_2/ErGO/GCE were removed by ten successive scans of cyclic voltammograms in 0.1 M PBS (pH=7.0). The anodic peak currents of 1.0 μM ponceau 4R and tartrazine keep 89.5% and 88.6% of their respective initial values after one-week storage (Figure S3), which demonstrated extraordinary storage stability.

3.7. Applications for Real Samples

The concentrations of ponceau 4R and tartrazine in orange juice samples were determined by the DPV technique using the TiO_2/ErGO/GCE. Orange juices were first diluted to 100-fold with 0.1 M PBS (pH = 7.0), then the DPV responses of ponceau 4R and tartrazine were recorded under the optimal experimental conditions. The concentrations of ponceau 4R and tartrazine were figured out from the related calibration curves. As tabulated in Table 2, the concentrations of ponceau 4R and tartrazine in orange juice were 0.112 (67.7 μg/L) and 0.423 μM (226 μg/L), respectively, which are much lower than their maximum allowable dosages (100 mg/L) specified in GB 2760–2014. To further confirm the detection reliability, known concentration solutions of ponceau 4R and tartrazine were separately spiked to the sample solutions. The satisfactory recoveries were obtained in the recovery assays with the accepted RSDs. These results suggest that the TiO_2/ErGO/GCE could obtain reliable detection results without visible interference from the complicated matrix. The promising analytical properties, along with low cost, simple fabrication, and facile operation, were expected to broaden the application prospects of TiO_2/ErGO/GCE.

Table 2. Detection of ponceau 4R and tartrazine in soft drink samples by the TiO_2/ErGO/GCE.

Samples	Analytes	Detected (μM)	RSD (%)	Added (μM)	Found (μM)	RSD (%)	Recovery (%)
A	Ponceau 4R	0.112	4.04	0.090	0.197	3.02	94.4
	Tartrazine	0.423	2.21	0.338	0.654	3.04	97.9
B	Ponceau 4R	0.112	3.21	0.112	0.223	4.06	99.1
	Tartrazine	0.423	5.01	0.583	1.056	4.86	108.6

4. Conclusions

A simple but efficient voltammetric sensor was constructed for the simultaneous detection of ponceau 4R and tartrazine based on TiO_2/ErGO composites. TiO_2 NPs were uniformly anchored on the ErGO nanoflakes, which provide a favorable electrode interface for the electrochemical oxidation of target species. Electrochemical experiments show TiO_2/ErGO composites decreased charge transfer resistance and enlarged the effective electrochemical active area significantly. The TiO_2/ErGO/GCE generated a synergistic enhancement effect for the electrooxidation of ponceau 4R and tartrazine, which gave a rise in greatly amplified voltammetric responses. Compared with bare GCE, the anodic

peak currents increased by 5-fold and 9-fold for ponceau 4R and tartrazine, respectively. Under the optimal analytical conditions, the TiO_2/ErGO/GCE achieved sensitive determination of ponceau 4R and tartrazine at the nanomolar level, with the low LODs of 4.0 and 6.0 nM for ponceau 4R and tartrazine over a wide dynamical response range (0.01−0.50 μM). Finally, the proposed TiO_2/ErGO/GCE enabled simultaneous determination of ponceau 4R and tartrazine in orange juices with a satisfactory outcome. Combined with portable electrochemical devices, the proposed TiO_2/ErGO/GCE is expected to achieve in-situ detection of azo colorants in various drinks and foodstuffs.

Supplementary Materials: The following are available online at http://www.mdpi.com/2227-9040/8/3/70/s1, Figure S1: Cyclic voltammograms of ponceau 4R (A) and tartrazine (B) at various scan rates, Figure S2: Anodic AdSDPV peak currents of ponceau 4R and tartrazine parallelly recorded on five TiO_2/ErGO/GCEs, Figure S3: AdSDPVs responses of ponceau 4R and tartrazine in dependence on storage time, Table S1: Anodic peak currents of ponceau 4R and tartrazine in the presence of various interfering substances.

Author Contributions: Conceptualization, Z.Q. and J.Z.; methodology, Z.Q. and J.Z.; formal analysis, Z.Q., J.Z. and J.L.; investigation, Z.Q., J.Z., Y.L. and J.W.; writing—original draft preparation, Z.Q. and J.Z.; writing—review and editing, G.L.; visualization, Z.Q., J.Z., Y.L. and J.W.; supervision, G.L. and Q.H.; funding acquisition, G.L. All authors have read and agreed to the published version of the manuscript.

Funding: This work was financially supported by Scientific Research Foundation of Hunan Provincial Education Department (18C0522), Undergraduates' Innovation Experiment Program of Hunan Province (2018649), Natural Science Foundation of Hunan Province (2018JJ3134), and National Natural Science Foundation of China (61703152).

Conflicts of Interest: The authors declare no conflict of interest.

References

1. Yoshioka, N.; Ichihashi, K. Determination of 40 synthetic food colors in drinks and candies by high performance liquid chromatography using a short column with photodiode array detection. *Talanta* **2008**, *74*, 1408–1413. [CrossRef]
2. Tanaka, T. Reproductive and neurobehavioural toxicity study of Ponceau 4R administered to mice in the diet. *Food Chem. Toxicol.* **2006**, *44*, 1651–1658. [CrossRef]
3. Tanaka, T. Reproductive and neurobehavioural toxicity study of tartrazine administered to mice in the diet. *Food Chem. Toxicol.* **2006**, *44*, 179–187. [CrossRef]
4. Sun, H.; Sun, N.; Li, H.; Zhang, J.; Yang, Y. Development of multiresidue analysis for 21 synthetic colorants in meat by microwave–assisted extraction–solid–phase extraction–reversed–phase ultrahigh performance liquid chromatography. *Food Anal. Methods* **2013**, *6*, 1291–1299. [CrossRef]
5. EFSA Panel on Food Additives and Nutrient Sources added to Food (ANS). Scientific Opinion on the re–evaluation Tartrazine (E 102). *EFSA J.* **2009**, *7*, 1331. [CrossRef]
6. EFSA Panel on Food Additives and Nutrient Sources added to Food (ANS). Scientific Opinion on the re–evaluation of Ponceau 4R (E 124) as a food additive. *EFSA J.* **2009**, *7*, 1328. [CrossRef]
7. Huang, H.-Y.; Shih, Y.-C.; Chen, Y.-C. Determining eight colorants in milk beverages by capillary electrophoresis. *J. Chromatogr.* **2002**, *959*, 317–325. [CrossRef]
8. Chou, S.S.; Lin, Y.H.; Cheng, C.C.; Hwang, D.F. Determination of synthetic colors in soft drinks and confectioneries by micellar electrokinetic capillary chromatography. *J. Food Sci.* **2002**, *67*, 1314–1318. [CrossRef]
9. Altınöz, S.; Toptan, S. Determination of Tartrazine and Ponceau–4R in various food samples by Vierordt's method and ratio spectra first–order derivative UV spectrophotometry. *J. Food Compost. Anal.* **2002**, *15*, 667–683. [CrossRef]
10. Capitán-Vallvey, L.; Fernández, M.; De Orbe, I.; Avidad, R. Simultaneous determination of the colorants tartrazine, ponceau 4R and sunset yellow FCF in foodstuffs by solid phase spectrophotometry using partial least squares multivariate calibration. *Talanta* **1998**, *47*, 861–868. [CrossRef]
11. García-Falcón, M.S.; Simal-Gándara, J. Determination of food dyes in soft drinks containing natural pigments by liquid chromatography with minimal clean–up. *Food Control* **2005**, *16*, 293–297. [CrossRef]
12. Bonan, S.; Fedrizzi, G.; Menotta, S.; Elisabetta, C. Simultaneous determination of synthetic dyes in foodstuffs and beverages by high–performance liquid chromatography coupled with diode–array detector. *Dyes Pigments* **2013**, *99*, 36–40. [CrossRef]

13. Liao, Q.G.; Li, W.H.; Luo, L.G. Applicability of accelerated solvent extraction for synthetic colorants analysis in meat products with ultrahigh performance liquid chromatography–photodiode array detection. *Anal. Chim. Acta* **2012**, *716*, 128–132. [CrossRef] [PubMed]
14. López-de-Alba, P.L.; López-Martínez, L.; De-León-Rodríguez, L.M. Simultaneous determination of synthetic dyes tartrazine, allura red and sunset yellow by differential pulse polarography and partial least squares. A multivariate calibration method. *Electroanalysis* **2002**, *14*, 197–205. [CrossRef]
15. Chanlon, S.; Joly-Pottuz, L.; Chatelut, M.; Vittori, O.; Cretier, J.L. Determination of carmoisine, allura red and ponceau 4R in sweets and soft drinks by differential pulse polarography. *J. Food Compost. Anal.* **2005**, *18*, 503–515. [CrossRef]
16. Combeau, S.; Chatelut, M.; Vittori, O. Identification and simultaneous determination of Azorubin, Allura red and Ponceau 4R by differential pulse polarography: Application to soft drinks. *Talanta* **2002**, *56*, 115–122. [CrossRef]
17. Huang, J.; Zeng, Q.; Wang, L. Ultrasensitive electrochemical determination of Ponceau 4R with a novel ε–MnO_2 microspheres/chitosan modified glassy carbon electrode. *Electrochim. Acta* **2016**, *206*, 176–183. [CrossRef]
18. Wang, Z.; Zhang, H.; Wang, Z.; Zhang, J.; Duan, X.; Xu, J.; Wen, Y. Trace analysis of Ponceau 4R in soft drinks using differential pulse stripping voltammetry at SWCNTs composite electrodes based on PEDOT:PSS derivatives. *Food Chem.* **2015**, *180*, 186–193. [CrossRef]
19. Zhang, Y.; Zhang, X.; Lu, X.; Yang, J.; Wu, K. Multi–wall carbon nanotube film–based electrochemical sensor for rapid detection of Ponceau 4R and Allura Red. *Food Chem.* **2010**, *122*, 909–913. [CrossRef]
20. Gan, T.; Sun, J.; Meng, W.; Song, L.; Zhang, Y. Electrochemical sensor based on graphene and mesoporous TiO_2 for the simultaneous determination of trace colourants in food. *Food Chem.* **2013**, *141*, 3731–3737. [CrossRef]
21. Ghoreishi, S.M.; Behpour, M.; Golestaneh, M. Simultaneous determination of Sunset yellow and Tartrazine in soft drinks using gold nanoparticles carbon paste electrode. *Food Chem.* **2012**, *132*, 637–641. [CrossRef] [PubMed]
22. Ye, X.; Du, Y.; Lu, D.; Wang, C. Fabrication of β–cyclodextrin–coated poly (diallyldimethylammonium chloride)–functionalized graphene composite film modified glassy carbon–rotating disk electrode and its application for simultaneous electrochemical determination colorants of sunset yellow and tartrazine. *Anal. Chim. Acta* **2013**, *779*, 22–34. [PubMed]
23. Zhang, W.; Liu, T.; Zheng, X.; Huang, W.; Wan, C. Surface–enhanced oxidation and detection of Sunset Yellow and Tartrazine using multi–walled carbon nanotubes film–modified electrode. *Colloids Surf. B* **2009**, *74*, 28–31. [CrossRef]
24. Yang, X.; Qin, H.; Gao, M.; Zhang, H. Simultaneous detection of Ponceat 4R and tartrazine in food using adsorptive stripping voltammetry on an acetylene black nanoparticle–modified electrode. *J. Sci. Food Agric.* **2011**, *91*, 2821–2825. [CrossRef] [PubMed]
25. Zhang, J.; Wang, X.; Zhang, S.; Wang, W.; Hojo, M.; Chen, Z. An electrochemical sensor for simultaneous determination of ponceau 4R and tartrazine based on an ionic liquid modified expanded graphite paste electrode. *J. Electrochem. Soc.* **2014**, *161*, H453–H457. [CrossRef]
26. Wang, M.; Zhao, J. A facile method used for simultaneous determination of ponceau 4R, allura red and tartrazine in alcoholic beverages. *J. Electrochem. Soc.* **2015**, *162*, H321–H327. [CrossRef]
27. He, Q.; Liu, J.; Liu, X.; Li, G.; Deng, P.; Liang, J.; Chen, D. Sensitive and selective detection of tartrazine based on TiO_2–electrochemically reduced graphene oxide composite–modified electrodes. *Sensors* **2018**, *18*, 1911. [CrossRef]
28. Zhou, W.-Y.; Liu, J.-Y.; Song, J.-Y.; Li, J.-J.; Liu, J.-H.; Huang, X.-J. Surface–electronic–state–modulated, single–crystalline (001) TiO_2 nanosheets for sensitive electrochemical sensing of heavy–metal ions. *Anal. Chem.* **2017**, *89*, 3386–3394. [CrossRef]
29. Shehata, M.; Azab, S.; Fekry, A.; Ameer, M.A. Nano–TiO_2 modified carbon paste sensor for electrochemical nicotine detection using anionic surfactant. *Biosens. Bioelectron.* **2016**, *79*, 589–592. [CrossRef]
30. Bao, S.J.; Li, C.M.; Zang, J.F.; Cui, X.Q.; Qiao, Y.; Guo, J. New nanostructured TiO_2 for direct electrochemistry and glucose sensor applications. *Adv. Funct. Mater.* **2008**, *18*, 591–599. [CrossRef]
31. Fan, Y.; Huang, K.-J.; Niu, D.-J.; Yang, C.-P.; Jing, Q.-S. TiO_2–graphene nanocomposite for electrochemical sensing of adenine and guanine. *Electrochim. Acta* **2011**, *56*, 4685–4690. [CrossRef]

32. Benvenuto, P.; Kafi, A.; Chen, A. High performance glucose biosensor based on the immobilization of glucose oxidase onto modified titania nanotube arrays. *J. Electroanal. Chem.* **2009**, *627*, 76–81. [CrossRef]
33. Daniel, D.; Gutz, I.G. Microfluidic cell with a TiO_2–modified gold electrode irradiated by an UV–LED for in situ photocatalytic decomposition of organic matter and its potentiality for voltammetric analysis of metal ions. *Electrochem. Commun.* **2007**, *9*, 522–528. [CrossRef]
34. Wan, X.; Yang, S.; Cai, Z.; He, Q.; Ye, Y.; Xia, Y.; Li, G.; Liu, J. Facile synthesis of MnO_2 nanoflowers/N–doped reduced graphene oxide composite and its application for simultaneous determination of dopamine and uric acid. *Nanomaterials* **2019**, *9*, 847. [CrossRef]
35. Cai, Z.; Ye, Y.; Wan, X.; Liu, J.; Yang, S.; Xia, Y.; Li, G.; He, Q. Morphology–dependent electrochemical sensing properties of iron oxide–graphene oxide nanohybrids for dopamine and uric acid. *Nanomaterials* **2019**, *9*, 835. [CrossRef]
36. He, Q.; Liu, J.; Liu, X.; Li, G.; Chen, D.; Deng, P.; Liang, J. A promising sensing platform toward dopamine using MnO_2 nanowires/electro–reduced graphene oxide composites. *Electrochim. Acta* **2019**, *296*, 683–692. [CrossRef]
37. Li, G.; Xia, Y.; Tian, Y.; Wu, Y.; Liu, J.; He, Q.; Chen, D. Recent developments on graphene–based electrochemical sensors toward nitrite. *J. Electrochem. Soc.* **2019**, *166*, B881–B895. [CrossRef]
38. Li, Q.; Xia, Y.; Wan, X.; Yang, S.; Cai, Z.; Ye, Y.; Li, G. Morphology–dependent MnO_2/nitrogen–doped graphene nanocomposites for simultaneous detection of trace dopamine and uric acid. *Mater. Sci. Eng. C* **2020**, *109*, 110615. [CrossRef]
39. Li, G.; Zhong, P.; Ye, Y.; Wan, X.; Cai, Z.; Yang, S.; Xia, Y.; Li, Q.; Liu, J.; He, Q. A highly sensitive and stable dopamine sensor using shuttle–like α–Fe_2O_3 nanoparticles/electro–reduced graphene oxide composites. *J. Electrochem. Soc.* **2019**, *166*, B1552–B1561. [CrossRef]
40. Kamat, P.V. Graphene–based nanoarchitectures. Anchoring semiconductor and metal nanoparticles on a two–dimensional carbon support. *J.Phys.Chem. Lett.* **2009**, *1*, 520–527. [CrossRef]
41. Fan, Y.; Lu, H.-T.; Liu, J.-H.; Yang, C.-P.; Jing, Q.-S.; Zhang, Y.-X.; Yang, X.-K.; Huang, K.-J. Hydrothermal preparation and electrochemical sensing properties of TiO_2–graphene nanocomposite. *Colloids Surf. B* **2011**, *83*, 78–82. [CrossRef] [PubMed]
42. Jang, H.D.; Kim, S.K.; Chang, H.; Roh, K.-M.; Choi, J.-W.; Huang, J. A glucose biosensor based on TiO_2–graphene composite. *Biosens. Bioelectron.* **2012**, *38*, 184–188. [CrossRef] [PubMed]
43. Fan, Y.; Liu, J.-H.; Lu, H.-T.; Zhang, Q. Electrochemistry and voltammetric determination of L–tryptophan and L–tyrosine using a glassy carbon electrode modified with a Nafion/TiO_2–graphene composite film. *Microchim. Acta* **2011**, *173*, 241–247. [CrossRef]
44. Park, S.; Ruoff, R.S. Chemical methods for the production of graphenes. *Nat. Nanotechnol.* **2009**, *4*, 217.
45. Gan, T.; Shi, Z.; Deng, Y.; Sun, J.; Wang, H. Morphology–dependent electrochemical sensing properties of manganese dioxide–graphene oxide hybrid for guaiacol and vanillin. *Electrochim. Acta* **2014**, *147*, 157–166. [CrossRef]
46. Tang, Y.-B.; Lee, C.-S.; Xu, J.; Liu, Z.-T.; Chen, Z.-H.; He, Z.; Cao, Y.-L.; Yuan, G.; Song, H.; Chen, L. Incorporation of graphenes in nanostructured TiO_2 films via molecular grafting for dye–sensitized solar cell application. *ACS Nano* **2010**, *4*, 3482–3488. [CrossRef]
47. Lambert, T.N.; Chavez, C.A.; Hernandez-Sanchez, B.; Lu, P.; Bell, N.S.; Ambrosini, A.; Friedman, T.; Boyle, T.J.; Wheeler, D.R.; Huber, D.L. Synthesis and characterization of titania−graphene nanocomposites. *J. Phys. Chem. C* **2009**, *113*, 19812–19823. [CrossRef]
48. Luo, X.; Morrin, A.; Killard, A.J.; Smyth, M.R. Application of nanoparticles in electrochemical sensors and biosensors. *Electroanal* **2006**, *18*, 319–326. [CrossRef]
49. He, Q.; Liu, J.; Liu, X.; Li, G.; Deng, P.; Liang, J. Manganese dioxide nanorods/electrochemically reduced graphene oxide nanocomposites modified electrodes for cost–effective and ultrasensitive detection of Amaranth. *Colloids Surf. B* **2018**, *172*, 565–572. [CrossRef]
50. Li, G.; Wang, S.; Duan, Y.Y. Towards conductive–gel–free electrodes: Understanding the wet electrode, semi–dry electrode and dry electrode–skin interface impedance using electrochemical impedance spectroscopy fitting. *Sens. Actuators B Chem.* **2018**, *277*, 250–260. [CrossRef]
51. Li, G.; Wu, J.; Xia, Y.; Wu, Y.; Tian, Y.; Liu, J.; Chen, D.; He, Q. Towards emerging EEG applications: A novel printable flexible Ag/AgCl dry electrode array for robust recording of EEG signals at forehead sites. *J. Neural Eng.* **2020**, *17*, 026001. [CrossRef] [PubMed]

52. Fan, Y.; Liu, J.-H.; Lu, H.-T.; Zhang, Q. Electrochemical behavior and voltammetric determination of paracetamol on Nafion/TiO_2–graphene modified glassy carbon electrode. *Colloids Surf. B* **2011**, *85*, 289–292. [CrossRef] [PubMed]
53. Laviron, E. General expression of the linear potential sweep voltammogram in the case of diffusionless electrochemical systems. *J. Electroanal. Chem.* **1979**, *101*, 19–28. [CrossRef]
54. Zhang, Y.; Hu, L.; Liu, X.; Liu, B.; Wu, K. Highly–sensitive and rapid detection of ponceau 4R and tartrazine in drinks using alumina microfibers–based electrochemical sensor. *Food Chem.* **2015**, *166*, 352–357. [CrossRef] [PubMed]
55. Cheng, Q.; Xia, S.; Tong, J.; Wu, K. Highly–sensitive electrochemical sensing platforms for food colourants based on the property–tuning of porous carbon. *Anal. Chim. Acta* **2015**, *887*, 75–81. [CrossRef]